Effect of Cooling Rate on Microstructure and Fracture Characteristics of β-Rich α + β Type Ti-4.5Al-3V-2Mo-2Fe Alloy

Materials Transactions, Vol. 42, No. 7 (2001) pp. 1339 to 1348

Effect of Cooling Rate on Microstructure and Fracture Characteristics of β-Rich $\alpha + \beta$ Type Ti–4.5Al–3V–2Mo–2Fe Alloy

Gunawarman[1, *1], Mitsuo Niinomi[1], Kei-ichi Fukunaga[1], Daniel Eylon[2], Shiro Fujishiro[3], and Chiaki Ouchi[4, *2]

[1]*Department of Production Systems Engineering, Toyohashi University of Technology, Toyohashi 441-8580, Japan*
[2]*Graduate Materials Engineering, University of Dayton, 300 College Park, Dayton, OH 45469-0240, USA*
[3]*Former Asian Office of Aerospace R & D, US Air Force Office of Scientific Research, Tokyo 106-0032, Japan*
[4]*Materials and Processing Research Center, NKK Co., Japan*

This study investigated the effect of cooling rate on microstructure and fracture characteristics of β-rich $\alpha + \beta$ type Ti–4.5Al–3V–2Mo–2Fe alloy rolled plate. Particular attention was paid to the roles of the local and continuous secondary phases within prior β grain in the static fracture toughness. A variety of microstructures containing different types, morphologies, sizes and volume fractions of secondary phases were obtained in matrix β (within prior β grain) with varying cooling rates; namely, water-quenching (WQ), air-cooling (AC), furnace-cooling (FC) and slow furnace-cooling (SFC) from various solutionizing temperatures in the $\alpha + \beta$ field. The types of secondary phases are martensite α (orthorhombic α''), acicular α and plate-like α observed in WQ, AC and FC specimens, respectively. While, there is no or lack secondary phase observed in matrix β for SFC specimen. Deformation-induced martensite (α''), DIM, was observed in WQ specimens after testing. The results showed that the fracture toughness, J_{IC}, and calculated flow stress, σ_f, of the microstructures containing a secondary phase depend mainly on the type and width of the secondary phase. The J_{IC} of microstructures containing a secondary phase, in general, is superior to that of the microstructures lacking secondary phases. Both the martensite α and DIM appear to increase J_{IC}. In a particular condition, J_{IC} decreases slightly with increasing width of acicular α for microstructure containing predominantly local acicular α, but increases monotonously with further increases in the width of acicular α. J_{IC} increases considerably with increasing width of plate-like α. The increase of J_{IC} is mainly due to increasing the effect of extrinsic toughening mechanism.

(Received January 9, 2001; Accepted May 7, 2001)

Keywords: *fracture characteristic, fracture toughness, microstructure, secondary phase, β-rich $\alpha + \beta$ titanium alloy, Ti–4.5Al–3V–2Mo–2Fe*

1. Introduction

The term secondary phase in this study refers to the local or continuous structure within prior β grain that appears during cooling from solutionizing temperature in $\alpha + \beta$ field. For conventional $\alpha + \beta$ titanium alloys such as Ti–6Al–4V, it is well understood that cooling at different rates from the two-phase field produces different types of secondary phases. Water-cooling and air-cooling treatments produce martensite α (hexagonal α' or orthorhombic α'') and acicular α (sometimes called secondary α or lamellar α), respectively. While furnace-cooling treatment produces β phase in the form of intergranular structure.[1)] The intergranular β phase generally lacks a secondary phase.

Many authors have investigated the effects of a secondary phase on the mechanical properties of $\alpha + \beta$ titanium alloys. Thus, the effect of a secondary phase on tensile properties is well understood. The relatively hard acicular α phase can act as a barrier against dislocations,[2)] thus tensile strength increases but elongation decreases with increasing volume fraction of acicular α phase.[2–4)] While, the relatively soft martensite α (α'') gives low yield stress and high ductility.[1,5,6)] On fracture toughness, however, the effect of a secondary phase is not well understood and the reports so far available are contradictory. Some authors[2,4,7)] have reported the acicular α decreases fracture toughness. It was reported that the strain localization at α/β interfaces leads to early crack nucleation[2,7)] and does not allow the crack to become blunt,[2)] thus the acicular α decreases fracture toughness. On the other hand, some authors argue that the acicular α increases fracture toughness.[8–10)] It was shown that the crack deflects at some α/β interfaces, thus the acicular α increases crack path length and fracture toughness.[8)] Many authors[5,6,9)] reported that the occurrence of deformation induced martensite[5)] during testing leads to increase fracture toughness. The role of martensite α before testing on fracture toughness, therefore, is not clearly understood.

For β-rich $\alpha + \beta$ type Ti–4.5Al–3V–2Mo–2Fe alloy, Ishikawa *et al.*[11)] reported that water quenching and air-cooling treatment produces orthorhombic α'' and acicular α phases, respectively. On tensile properties, they found that the strength of this alloy, as well as that of the conventional $\alpha + \beta$ titanium alloy, decreases with decreasing cooling rates. It was also found that the strength of the alloy is relatively insensitive to cooling rate, and quench delay, *i.e.* the time elapsing from the extraction from a furnace to the start of quenching, than that of Ti–6Al–4V. It was explained that a highly stable β phase, as a result of high β stabilizer (Mo, Fe) contents in the alloy, suppresses diffusional transformation during cooling and quench delay. This also explains why furnaces cooling of the alloy from the two-phase field still produces a secondary phase, namely, plate-like α, as observed in our previous study.[12)] As for the fracture toughness, some authors reported that the fracture toughness K_{IC}[13–15)] or J_{IC}[16)] of the alloy conducted with air-cooling treatment decreases when the microstructure contains precipitated or fine acicular α, but increases when the microstructure contains coarse aci-

*1Graduate Student, Toyohashi University of Technology, Toyohashi 441-8580, Japan.
*2Present address: Graduate School of Engineering Tohoku University, Sendai 980-8579, Japan.

cular α. This indicates that the effect of an acicular α phase on fracture toughness depends on its size.

From the above analysis, it can be concluded that mechanical properties are quite sensitive to the formation of a secondary phase in $\alpha + \beta$ titanium alloys. The highly β stabilized Ti–4.5Al–3V–2Mo–2Fe alloy, which shows much more variety of secondary phases than that of conventional $\alpha+\beta$ titanium alloys, is expected to have a contribution in clarifying the effect of secondary phase on fracture toughness. For this purpose, various cooling rates from various annealing temperatures are used to adjust the type, size and amount of secondary phase in the Ti–4.5Al–3V–2Mo–2Fe alloy in order to investigate the effect of secondary phase on mechanical properties, in particular, fracture toughness.

2. Experimental Procedures

2.1 Material and heat treatment

The material used in this study was Ti–4.5Al–3V–2Mo–2Fe alloy in the form of 440 mm length × 160 mm width × 12.5 mm thick rolled plate. The alloy contained (by mass) 4.47%Al, 3.00%V, 1.86%Mo, 1.96%Fe, 0.1%O, 0.01%C, 0.01%N, 0.0036%H, and the balance being Ti. Rectangular blocks with the size of 55 mm length × 11 mm width × 11 mm thick were cut along the rolling direction of the plate. In order to get different types and sizes of secondary phases, the blocks were then solutionized at temperatures between 1103 K and 1173 K in $\alpha + \beta$ field for 3.6 ks followed by various cooling conditions, which were water-quenching (WQ), air-cooling (AC), furnace-cooling (FC) and slow furnace-cooling (SFC) treatments, respectively. Schematic illustrations of phase diagram and heat treatment schedules are presented in Fig. 1. Solution treatment was carried out in an evacuated quartz tube. The cooling rates for WQ, AC, FC, and SFC treatments were around 200 Ks^{-1}, 10 Ks^{-1}, 0.1 Ks^{-1}, and 0.05 Ks^{-1}, which were calculated by dividing half of the solutionizing temperature by the time required to reach that temperature on cooling.

2.2 Mechanical tests

Three point bending, 3 PB, fracture toughness test specimens with the size of 10 × 10 × 55 mm^3 were machined from the heat-treated blocks. The fatigue pre-crack was introduced into the slit tip for $a_o/W = 0.53$, where a_o and W are the initial crack length and the specimen width, respectively. The final geometry of specimens is shown in Fig. 2(a). The crack initiation point was detected using an AC electrical potential method as shown in Fig. 2(b). Static 3 PB fracture toughness tests were carried out using an Instron-type testing machine according to ASTM E813[17] at room temperature in air. Typical load-deflection curves resulting from fracture toughness tests of specimens for solutionizing temperature of 1173 K are shown in Fig. 3(a). The open marks on the curves indicate the crack initiation points.

The elastic plastic fracture toughness parameter at the crack initiation point, J_{in}, was calculated using the following equation;[18]

$$J_{in} = \frac{2A}{Bb}\left(\frac{1+\alpha}{1+\alpha^2}\right) \tag{1}$$

$$\alpha = \sqrt{(2a/b)^2 + 2(2a/b) + 2} - 2(a/b) + 1 \tag{2}$$

where A, a, B, and b are the area under load-deflection curve (see Fig. 3(a)), the crack length, the specimen thickness and the uncracked ligament length, respectively. Judging J_{in} with

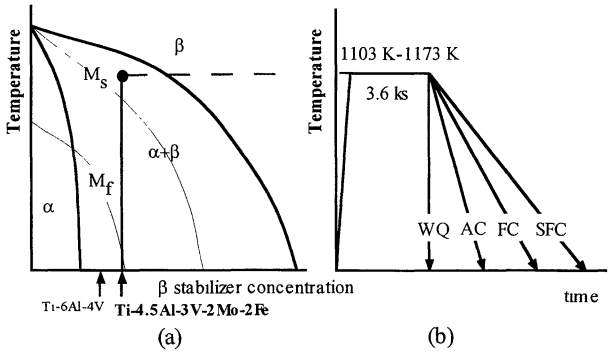

Fig. 1 Schematic illustrations of (a) phase diagram and (b) heat treatment schedules. WQ=water-quenching, AC=air-cooling, FC=furnace-cooling, and SFC=slow furnace-cooling.

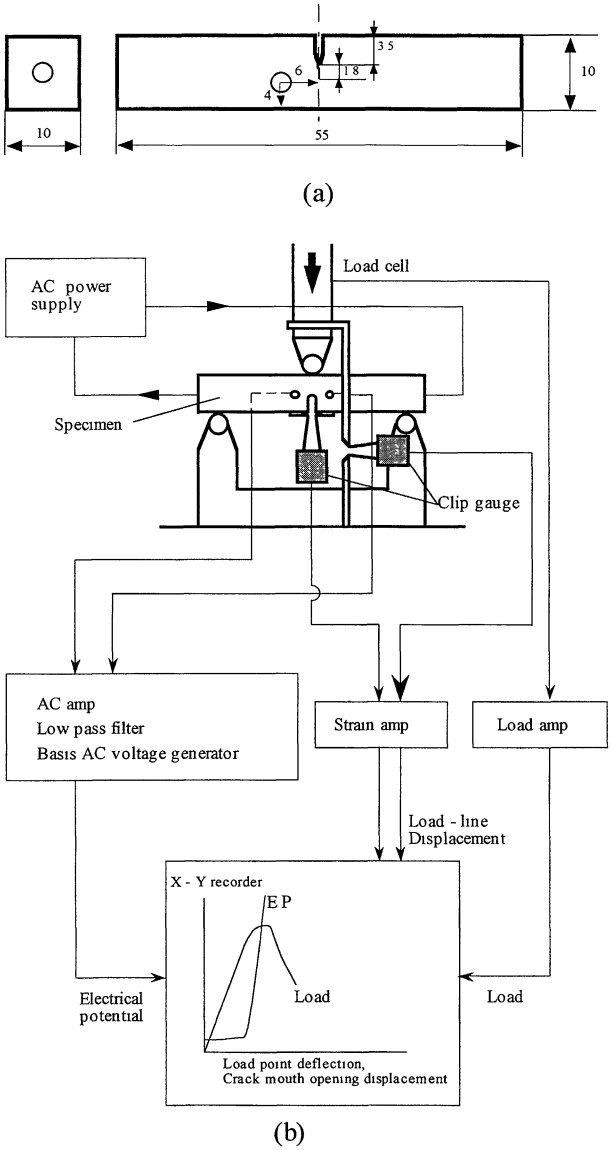

Fig. 2 Schematic illustrations of (a) geometry of fracture toughness specimen (in mm) and (b) fracture toughness test method.

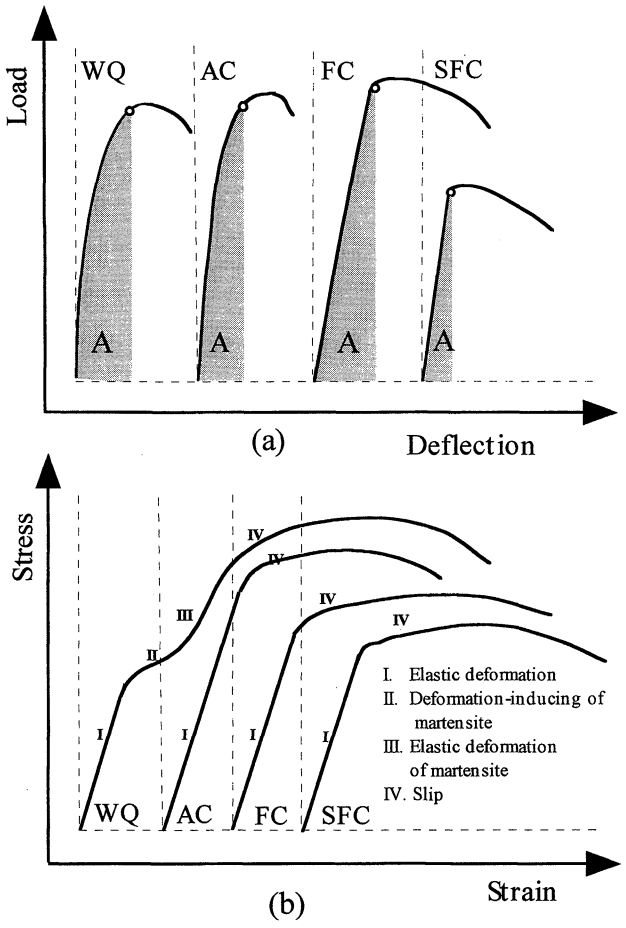

Fig. 3 Typical curves of (a) load-deflection of fracture toughness and (b) stress-strain of tensile tests for 1173 K specimen under the indicated cooling rates.

the following validity test conditions, then an approved elastic plastic fracture toughness value, namely, J_{IC} was determined.

$$a, b, B \geq 25\left(\frac{J_{in}}{\sigma_f}\right) \tag{3}$$

$$\sigma_f = \frac{\sigma_{0.2} + \sigma_B}{2} \tag{4}$$

where $\sigma_{0.2}$ and σ_B are the 0.2% proof stress and the tensile strength, respectively.

Tensile test specimens with a gauge diameter of 4 mm and a gauge length of 20 mm were used to measure tensile properties using an Instron-type testing machine at a cross head speed of 8.3×10^{-6} m/s at ambient temperature. An installed load cell in testing machine was used to detect the load. Both clip gauge and foil gauge directly attached to the specimens detected the strain. Typical stress-strain curves resulting from tensile tests of specimens for solutionizing temperature of 1173 K are shown in Fig. 3(b).

MicroVickers hardness tests were carried out on the same samples used for microstructural observations as is stated below with 10 s load for 15 s in order to measure hardness of primary α phase and prior β region (secondary phase+matrixβ).

2.3 Microstructural observations

Small samples with the size of $10 \times 10 \times 10\,mm^3$ for microstructural observations were taken from the fracture toughness tested specimens. The samples for optical microscopy, OM, and scanning electron microscopy, SEM, observations were ground, polished and then etched in solution of 5% nitric acid, 3% hydrofluoric acid and 92% water. Those for transmission electron microscopy, TEM, observations were ground and electropolished using a twin jet electropolishing unit at a temperature of 253 K in solution composed of 60% methanol, 30% butanol and 10% perchloric acid. The microstructural parameters, which are volume fraction and grain size (diameter) of primary α phase, volume fraction of prior β phase and prior β grain size (diameter), and volume fraction and size (width) of secondary phase, were measured from the SEM and TEM micrographs using an image analyzer. Fracture surface was observed using an SEM to characterize the fracture features and measure the stretched zone width, SZW. SZW was characterized by tilting the specimen 45° from the surface plane. The transverse cross section of the fracture surface was observed using an SEM in order to identify the crack path morphology and measure the effective crack propagation length (*i.e.* real crack propagation length), a_{eff}, per a certain nominal crack propagation length, a_n. A schematic diagram showing the fracture parameters is presented in Fig. 10(A).

X-ray diffraction (XRD) analysis was conducted using Cu–K_α under voltage and current conditions of 40 kV and 30 mA, respectively.

3. Experimental Results

3.1 Microstructures

Microstructures and mechanical properties of Ti–4.5Al–3V–2Mo–2Fe alloy for heat treatment conditions given in Fig. 1 are tabulated in Table 1. Typical SEM micrographs for solutionizing temperature of 1173 K under the given cooling rates are presented in Fig. 4. All microstructures contain primary α phase, α_p, (the dark phase in Fig. 4) and different types of secondary phase in matrix β (the bright phase in Fig. 4). α_p is found in the form of relatively globular (equiaxial) structures with an aspect ratio in the range of 1–2. Both the secondary phase and matrix β are found within prior β grain (some times called prior β phase or prior β region) as can be seen in Figs. 4(a)–(c). WQ specimens contain martensite α[1)] in matrix β (see Fig. 4(a)). XRD and TEM analysis showed that the structure of martensite α in WQ specimens is orthorhombic α″. This is consistent with that observed by Ishikawa *et al.*,[11)] that is, water quenched Ti–4.5Al–3V–2Mo–2Fe alloy (present alloy) solutionized above 1073 K contains orthorhombic α″. The type of matrix β was found as retained β, as commonly observed in water quenched α + β type titanium alloys.[1,11)] For convenience, the term of martensite α in matrix β will be used instead of orthorhombic α″ within matrix retained β hereafter. Microstructures of AC and FC specimens contain acicular α and plate-like α, respectively, in matrix β (see Figs. 4(b) and (c)). It was found that the plate-like α is derived from the previous acicular α. Microstructure of SFC specimen contains β phase that exists surrounding primary α phase (see Fig. 4(d)). This type of β phase is called as intergranular β phase[1)] and there is almost no secondary phase observed within this phase as can be seen in Fig. 4(d). Morphologies of the secondary phases were found predominantly in the form of local structure, mixture

Table 1 Heat treatment, mechanical properties and microstructures

Heat treatment		Mechanical properties				Microstructures
Solutionzing temperature, K	Cooling method	Tensile strength, MPa	0.2% proof stress, MPa	Elongation, %	Fracture toughness, kN/m	
1103	WQ	1028	903	16.5	33	α_p + martensite α in matrix β
	AC	987	912	13.2	34	α_p + acicular α in matrix β
	FC	951	938	17.0	41	α_p + plate-like α in matrix β
	SFC	948	901	16.3	14	α_p + intergranular β
1113	AC	1036	962	13.0	27	α_p + acicular α in matrix-β
1123	AC	1053	990	12.6	24	α_p + acicular α in matrix-β
1133	WQ	1152	602	17.8	47	α_p + martensite α in matrix β
	AC	1065	986	12.9	26	α_p + acicular α in matrix β
	FC	1002	894	16.7	55	α_p + plate-like α in matrix β
	SFC	930	892	16.1	19	α_p + intergranula β
1143	AC	1089	993	12.7	30	α_p + acicular α in matrix β
1173	WQ	1224	420	19.8	49	α_p + martensite α in matrix β
	AC	1053	986	9.4	42	α_p + acicular α in matrix β
	FC	961	882	17.8	105	α_p + plate-like α in matrix β
	SFC	946	888	15.2	27	α_p + intergranula β

WQ=water-quenching, AC=air-cooling, FC=furnace-cooling, SFC=slow furnace-cooling, α_p = primary α phase.

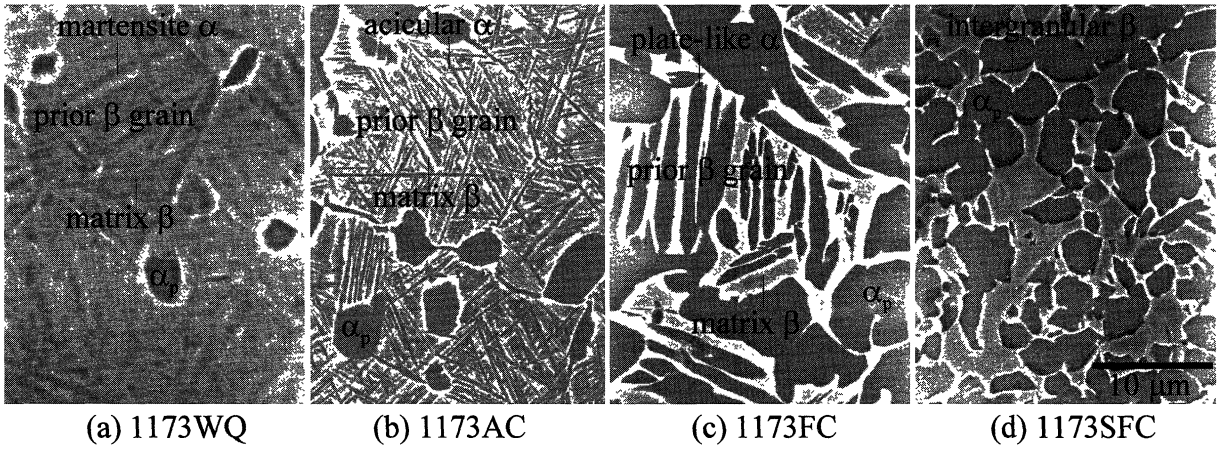

Fig. 4 Typical SEM micrographs of (a) 1173 WQ, (b) 1173 AC, (c) 1173 FC and (d) 1173 SFC specimens showing microstructures containing martensite α, acicular α, plate-like α and no secondary phase within matrix β, respectively.

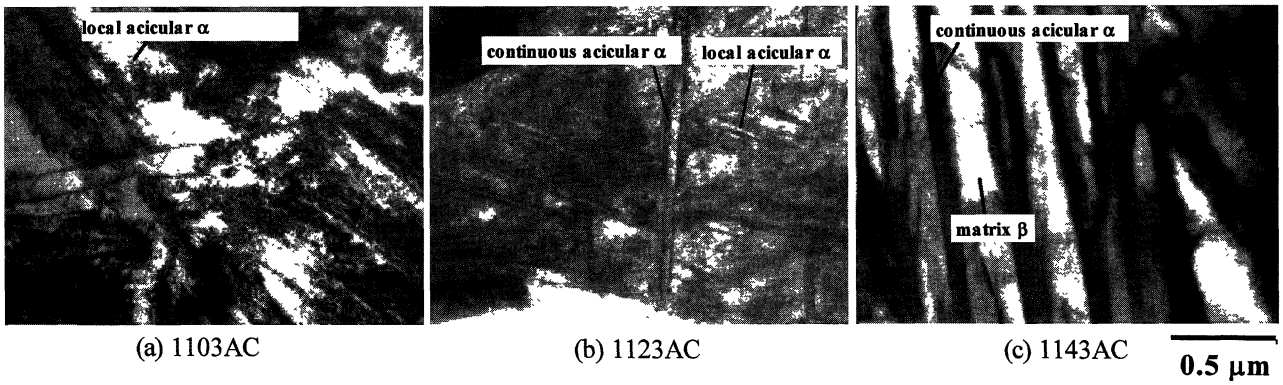

Fig. 5 Typical TEM micrographs of (a) 1103 AC, (b) 1123 AC and (c) 1143 AC specimens showing microstructures containing local, mixture of local and continuous, and continuous structures of acicular α, respectively.

of local and continuous structures and fully continuous structure according to the low (1103 K), intermediate (1133 K) and high (1173 K) solutionizing temperatures, respectively. Typical TEM micrographs showing microstructure containing acicular α in the form of local structure, mixture of local and continuous structures, and continuous structure are given in

Figs. 5(a), (b) and (c), respectively.

Microstructural parameters of the primary α, prior β and secondary phases were measured on SEM and TEM micrographs using an image analyzer. The parameters shown in Fig. 6 are the results of average analysis for three micrographs taken from different fields. Three conclusions can be drawn from the figure. That is, for the given cooling rate, (a) volume fraction of primary α phase decreases and volume fraction of prior β phase increases with increasing solutionizing temperature, (b) prior β grain size increases and grain size of primary α phase is nearly constant with increasing solutionizing temperature, and (c) volume fraction and size (width) of the secondary phase increase with increasing solutionizing temperature.

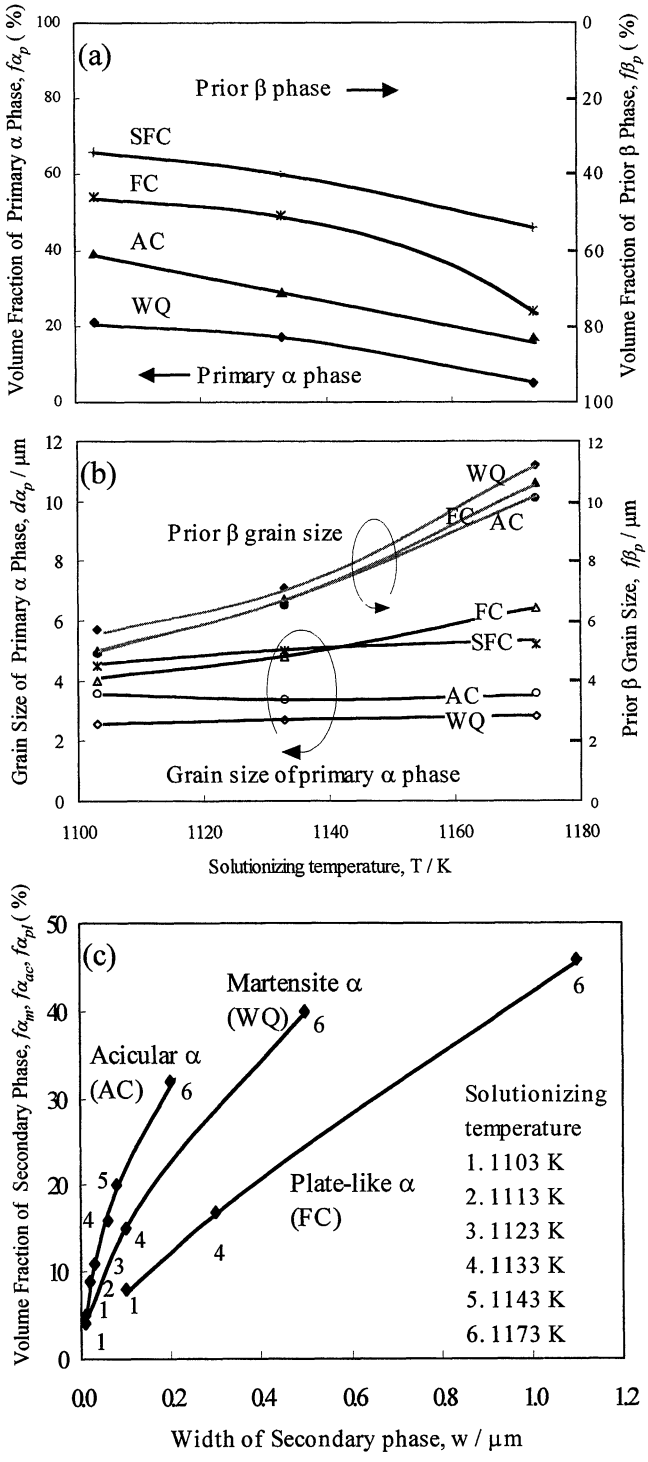

Fig. 6 Microstructural parameters; (a) volume fractions of primary α phase and prior β region, (b) grain size (diameter) of primary α phase and prior β grain size, and (c) volume fraction and width of secondary phase, respectively as a function of solutionizing temperature and cooling rate.

3.2 Mechanical properties

Mechanical properties; tensile strength, 0.2% proof stress, elongation and fracture toughness, of the alloy for the given solutionizing temperatures and cooling rates are tabulated in Table 1. Since, in the case of elastic plastic fracture mechanics, fracture toughness can be related to microstructural unit by using flow stress and strain rate,[9] the data in Table 1 are plotted in the form of fracture toughness, J_{IC}, against flow stress for the observed secondary phase (the given cooling rate) in Fig. 7. The flow stress, σ_f, was calculated by using eq. (4). The arrows indicate the direction of increasing solutionizing temperature and thus also indicate the direction

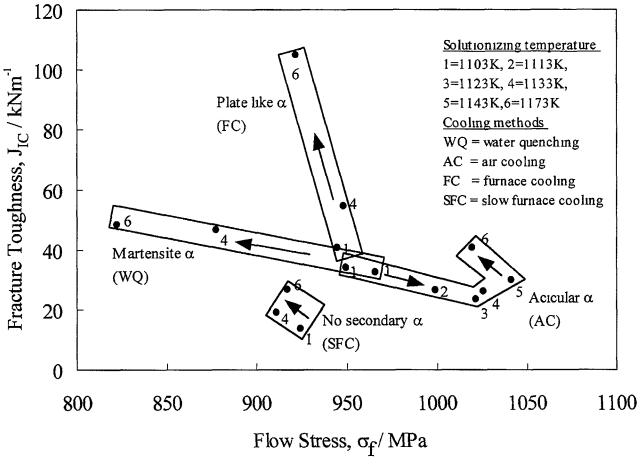

Fig. 7 Fracture toughness, J_{IC}, as a function of calculated flow stress, σ_f, for the microstructures containing indicated secondary phases type (the given cooling rate). Arrows indicate the direction of increasing solutionizing temperature as well as increasing volume fraction and width of secondary phase.

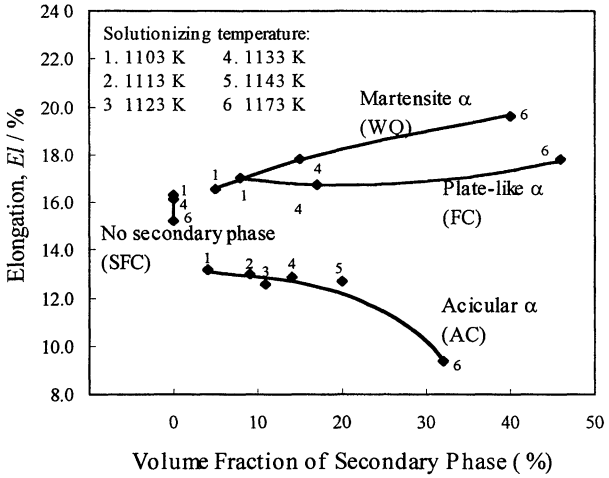

Fig. 8 Elongation, *El*, as a function of volume fraction of secondary phase for microstructures containing the indicated secondary phase type under the given cooling rate.

of increasing volume fraction or width of secondary phase as shown in Fig. 6(c). While the blocks indicate the trend of data for the given cooling rate. Elongation, El, is plotted against volume fraction of the secondary phase for the observed secondary phase (the given cooling rate) in Fig. 8. It is well known that the elongation is inversely related to the volume fraction of acicular α.[2–4)]

It is clearly shown in Fig. 7 that, for the microstructure containing martensite α (WQ), J_{IC} increases slightly from 33 to 47 kNm^{-1} while the σ_f decreases significantly from a level of 960 MPa to a level of 860 MPa with increasing solutionizing temperature. The decrease of σ_f, as a result of decreasing $\sigma_{0.2}$ (see Table 1), is mainly due to the deformation-induced martensite, DIM, a product of transformation process from retained β phase to martensite α during loading (straining). Microstructures of undeformed and deformed areas of tensile tested specimens can show the occurrence of DIM. That of 1133 WQ specimen, for example, is shown in Fig. 9. It can be seen that the amount of martensite phase (needle like phase in micrographs) is qualitatively much more in the deformed area (B and C) than that in the undeformed area (A). This reveals that DIM occurred in this specimen. Deformed areas of the other WQ specimens showed that 1173 WQ specimen has qualitatively much more DIM than 1133 WQ, but 1103 WQ specimen contains almost no DIM. This reveals that the DIM increases and, as a consequence, the $\sigma_{0.2}$ decreases with increasing solutionizing temperature. It is well known in titanium alloys that the DIM lowers yield stress (= $\sigma_{0.2}$), but increases ductility.[5,6)] It can be understood, therefore, why the elongation of 1133 WQ and 1173 WQ specimens is relatively higher, *i.e.* near 20% (Fig. 8). However, relatively higher elongation (around 16%) is also obtained for the 1103 WQ specimen and that the elongation appears to increase with increasing solutionizing temperature (Fig. 8) indicate that the martensite α (before testing) also contributes to increase the elongation in addition to that due to DIM.

For the microstructure containing acicular α (AC), it is seen in Fig. 7 that there exists three-steps of trends in the relationship between J_{IC} and σ_f with increasing solutionizing temperature. Firstly, J_{IC} decreases from 34 to 24 kNm^{-1}, while σ_o increases from a level of 950 MPa to a level of 1025 MPa when the observed microstructure contains local acicular α. Secondly, J_{IC} increases to 30 kNm^{-1}, while σ_f increases up to a level of 1050 MPa when the observed microstructure contains local and continuous acicular α. Thirdly, J_{IC} increases to 42 kNm^{-1} while σ_f decreases to a level of 1020 MPa when the observed microstructure contains continuous acicular α. Fig. 8 shows that the elongation decreases slightly from 13.2 to 12.7% with increasing volume fraction of acicular α when the observed microstructure contains local acicular α. But it decreases sharply up to 9.4% when the observed microstructure contains fully continuous acicular α. This indicates that the elongation decreases with the increase of volume fraction of acicular α and the decrement of elongation is more pronounced for microstructure containing continuous acicular α. This completely supports the finding of previous authors[19)] that the acicular α is a source of low ductility.

For the microstructure containing plate-like α (FC), Fig. 7 shows that J_{IC} increases significantly from 41 to 105 kNm^{-1}, while the σ_f decreases slightly from a level of 950 MPa to a level of 925 MPa with increasing solutionizing temperature. The elongation appears nearly independent of volume fraction of plate-like α and exists at a relatively high level *i.e.* around 17% (Fig. 8).

Fracture toughness of microstructures containing no secondary phase (SFC) measures between 14 and 27 kNm^{-1} and, in general, is lower than that of the microstructures containing a secondary phase (Fig. 7). The flow stress and elongation appear to be nearly constant at a level of around 920 MPa and 16%, respectively (Figs. 7 and 8). The relatively higher elongation in FC and SFC specimens, of which observed microstructures contain high volume fraction of coarse primary α phase (see Figs. 6(a) and (b)), indicates that the primary α phase takes a predominant part in controlling the elongation in both slowly cooled specimens.

3.3 Fracture morphologies

A schematic illustration of a transverse cross-section of the fractured specimen and typical photographs of the fracture surface and its cross-section at near crack tip are shown in Fig. 10. SZW and the ratio of a_{eff} and a_n (see Fig. 10(a)) were characterized in order to evaluate the contributions of crack tip blunting and crack deflection toughening, respectively, to the fracture toughness. SEM fractograph (Fig. 10(b)) shows fatigue pre-cracking, SZW and fracture surface regions. The fracture surface shows dimples indicating that

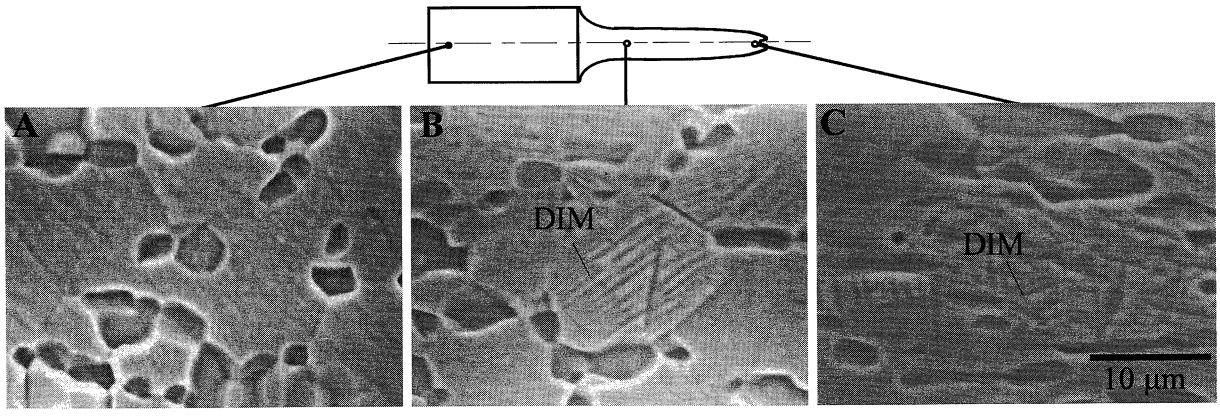

Fig. 9 SEM micrographs of undeformed (A), lightly deformed (B) and heavily deformed (C) regions of 1133 WQ tensile tested specimen showing deformation-induced martensite (DIM) in deformed regions (B and C).

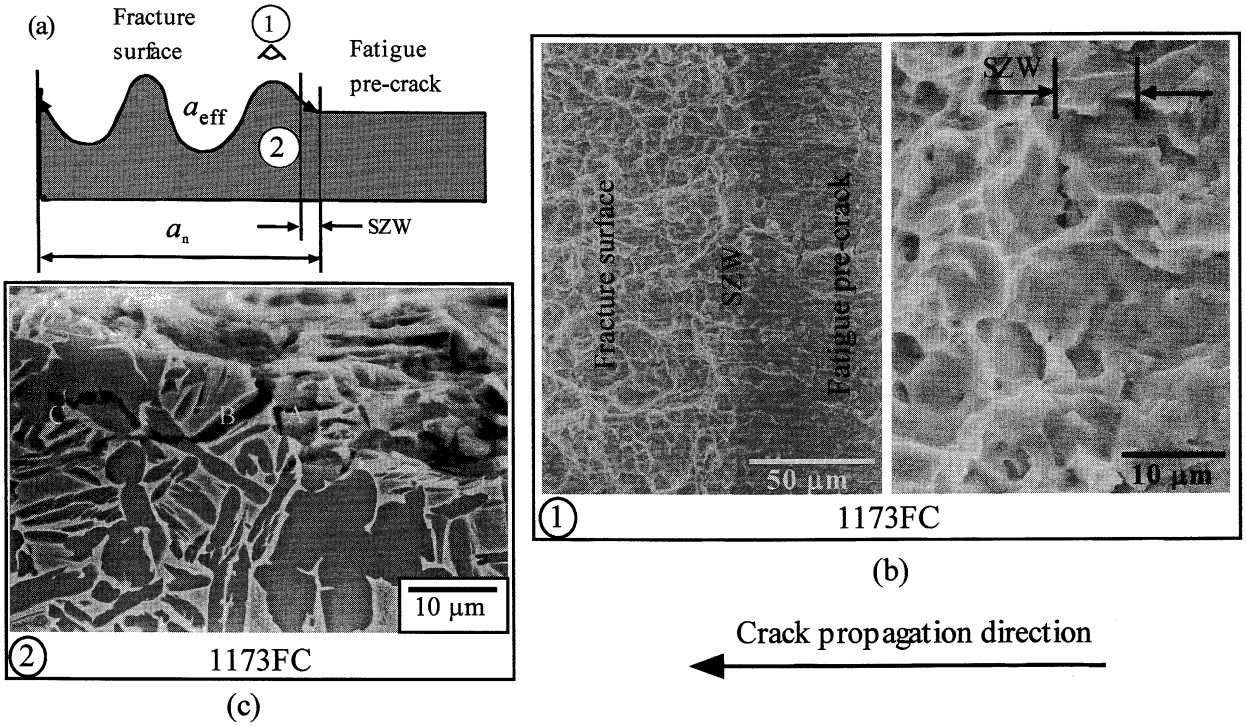

Fig. 10 (a) Schematic diagram of transverse cross-section of fractured specimen, and typical SEM photographs of (b) fracture surface and (c) transverse cross-section morphology of the fracture surface, respectively. A=crack deflection, B=crack branching, C=micro-cracking.

the failure mechanism is ductile fracture through void coalescence. The transverse cross section of the fracture surface of the 1173FC specimen (Fig. 10(c)) shows that the crack deflects and branches at some plate-like α phases.

Figure 11 shows the contribution of both crack tip blunting and crack deflection toughening mechanism to the fracture toughness, represented by the relative value of $J_{IC}/(\sigma_f\ SZW)$[12] (solid marks) and a_{eff}/a_n (open marks), respectively, for the observed secondary phase (the given cooling rate). The contribution of crack deflection (a_{eff}/a_n) in the microstructure lacking a secondary phase is small and no other toughening mechanisms are involved except crack tip blunting. This means that its fracture toughness is almost fully due to slipping deformation at the tip of fatigue pre-crack, which is known as the intrinsic toughening mechanism.[9] The contribution of crack tip blunting to the fracture toughness of the microstructure lacking a secondary phase is, therefore, nearly 1. It is seen that the relative contributions of crack tip blunting to fracture toughness of the microstructures containing martensite α, acicular α, and plate-like α phases are lower than 0.8 as indicated by the relative values of $J_{IC}/(\sigma_f\ SZW)$ in Fig. 11. This indicates that there exists an extrinsic toughening mechanism in the microstructures containing secondary phases in addition to the intrinsic one. Relatively high (a_{eff}/a_n) of the microstructure containing acicular α reveals that crack deflection gives a significant contribution to increasing its fracture toughness. Relatively higher fracture toughness for microstructure containing plate-like α, in particular, the coarse one is found to be due to micro cracking and crack branching (see Fig. 10(c)) in addition to the crack deflection (Fig. 11). While, for the microstructure containing martensite α, DIM partly contributes its fracture toughness.

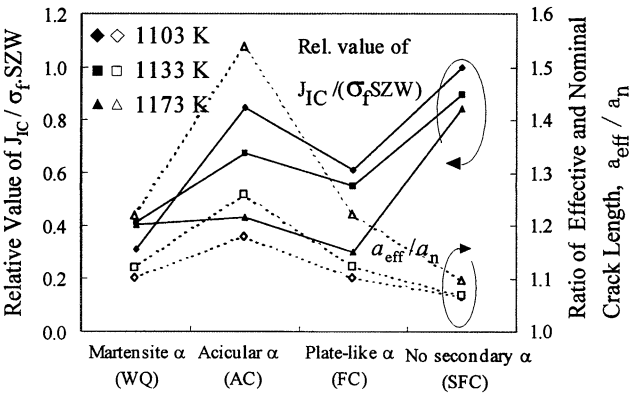

Fig. 11 Relative value of $J_{IC}/(\sigma_f$. SZW) and ratio of effective and nominal crack lengths, (a_{eff}/a_n) of microstructures containing indicated secondary phase type under the given cooling rate.

4. Discussion

The experimental results show that the fracture toughness of the microstructure lacking a secondary phase observed in SFC specimen, in general, is lower than that of the microstructures containing a secondary phase observed in WQ, AC and FC specimens (Fig. 7). In the cases of $\alpha + \beta$ type and near β type titanium alloys, some authors reported that the fracture toughness of furnace- or slow-cooled alloys is also low, but the reason for the lowering is likely quite different from that of the present alloy. Briggs *et al.*[20] found that the loss in the stress corrosion threshold (K_{ISCC}) in slow-cooled Ti–6V–4V ELI is due to the formation of intermetallic phase, α_2 (Ti_3Al). Bird *et al.*[21] reported that low fracture toughness

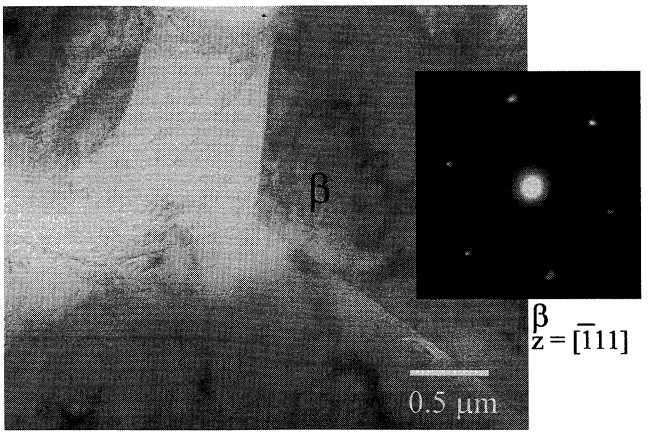

Fig. 12 TEM micrograph showing the absence of α_2 and ω phases in the 1173 SFC specimen.

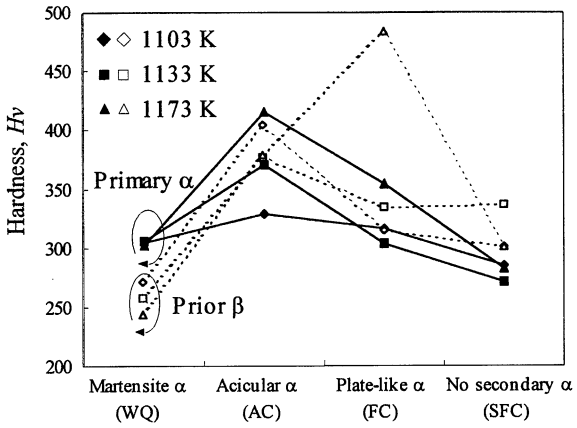

Fig. 13 Micro Vickers hardness of primary α phase and prior β region for microstructure containing indicated secondary phase type under the given cooling rate.

(K_{IC}) in the slow cooled Timetal-21s (Ti–15Mo–3Al–2.7Nb–0.25Si) alloy is related with the formation of ω phase. This indicates that the main reason for lowering fracture toughness for those type alloys is the presence of either a α_2 or an ω phase, which is well known as a hard and brittle phase.[1)] However, TEM analysis for the slow furnace-cooled specimen of the present alloy shows that there are no such phases characterized in the microstructure, as indicated by the TEM micrograph shown in Fig. 12. Selected area diffraction of β region shows only diffraction pattern of β phase. Since the presence of a hard phase in the microstructure usually increases the strength, the observed low tensile strength and high elongation for SFC specimen (see Table 1 or Fig. 7) can indirectly indicate the absence of α_2 and ω in the specimen. The result of micro Vickers hardness measurement (Fig. 13) shows that, for the microstructure lacking a secondary phase (SFC), the hardness of both a prior β region (intergranular β in this case) and a primary α phase is relatively low. This also indirectly indicates the absence of both hard phases in SFC specimen. The reasons for the absence of such phases or precipitates in the present alloy are due to its low content of α stabilizer (4.5%Al and 0.1%O) and β stabilizer (3.5%V, 2%Fe and 2%Mo). These factors seem to be effective in suppressing the formation of α_2 and ω phases, respectively during slow-cooling treatment. Therefore, it can be concluded that the low fracture toughness in the present alloy is not due to the presence of such brittle phases. The absence of a secondary phase like martensite α, acicular α or plate-like α within (intergranular) β phase, therefore, appears to be the main reason for the lowered fracture toughness in the present alloy. The absence of a secondary phase results in the absence of extrinsic toughening mechanism. As mentioned above, the fracture toughness of the microstructure lacking a secondary phase is almost fully contributed by the crack tip blunting effect (Fig. 11).

Figure 7 also shows that the fracture toughness and flow stress of the microstructures containing a local secondary phase (1103 WQ, 1103 AC and 1103 FC specimens) are almost the same. This indicates that the fracture toughness and flow stress are nearly independent of types and morphologies of the secondary phases when the volume fraction or width of the secondary phase is quite small. However, the fracture toughness and flow stress depend strongly on the types and

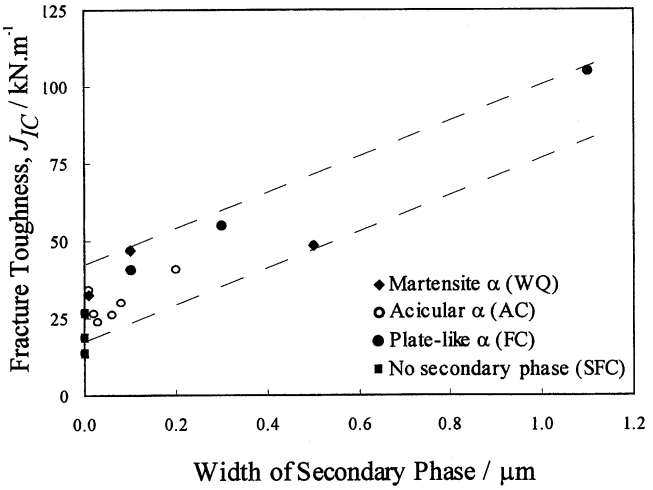

Fig. 14 Variation of fracture toughness, J_{IC}, as a function of width of secondary phase.

morphologies of the secondary phases when the volume fraction or width of the secondary phase increases. In order to show the dependence of fracture toughness on the width of the secondary phase, the related data is plotted in Fig. 14. It is clearly seen in this figure that the fracture toughness, in general, increases with the increasing width of the secondary phase. The increase of fracture toughness in the microstructures containing acicular α and plate-like α phases is found to be due to the increase of crack deflection (a_{eff}/a_n, Fig. 11). The increase of fracture toughness is more pronounced in the microstructure containing coarse acicular α or plate-like α phase due to increasing micro cracking and crack branching toughening mechanisms as observed in the 1173 FC specimen (Fig. 10(c)).

It is clearly seen in Fig. 7 and also in Fig. 14 that the presence of martensite α in WQ specimen increases the fracture toughness. The increase of fracture toughness is more pronounced when the observed microstructure contains DIM (1133 WQ and 1173 WQ specimens). This indicates that both martensite α and DIM contribute to increase fracture toughness of WQ specimen. The increase of fracture toughness due to martensite α (before testing) is suggested to be re-

lated with the high damping capacity of martensite α (α'').[22] The martensite α phase would absorb a part of energy and, as a consequence, much more the energy would be needed for crack tip opening, and thus martensite α would increase the fracture toughness. While, stored energy for the transformation of retained β to martensite α during deformation is believed to be the main reason for the increase of fracture toughness due to DIM.[13] However, the increase in fracture toughness is the result of significant decrease in the 0.2% proof stress (yield stress). Figure 13 shows that, for martensite α (WQ), the hardness of prior β region (martensite α + matrix retained β) is low and decreases with increasing volume fraction of martensite α (as a result of increasing solutionizing temperature). This clearly indicates that the martensite α phase has low hardness. The presence of high volume fraction of the soft martensite β (before testing) is also, therefore, one reason for the lowering the yield stress, high elongation (Fig. 8), and high work hardening rate (see Fig. 3(b) for WQ) in addition to DIM. It is well known in $\alpha+\beta$ titanium alloys that water quenched alloy produces such properties when DIM transformation occurs.[5,6]

It was explained in our previous report[16] that the effect of acicular α on fracture toughness of the microstructure containing acicular α depends on its size (width). The presence of acicular α within the prior β grain provides a much larger interface phase, a source of void nucleation and internal stress, in the microstructure. It causes the crack to propagate easily within prior β grain. Fine acicular α will be cut by cracks, but coarse acicular α has to be bypassed. Thus, coarse acicular α will increase fracture toughness as a result of increasing crack deflection effect ($a_{\mathrm{eff}}/a_{\mathrm{n}}$). In addition, the present results show that the fracture toughness of the specimen having the microstructure containing acicular α also depends on the morphology of acicular α. As mentioned above, with increasing width of acicular α, the fracture toughness decreases slightly for the microstructure containing local acicular α. On the other hand, the fracture toughness increases for the microstructure containing continuous acicular α. The decrease of fracture toughness in the microstructure containing local acicular α is mainly due to the decrement of crack tip blunting effect (see Fig. 11) as a result of the presence of many more α/β interfaces in the microstructure. While, the increase of fracture toughness in the microstructure containing continuous acicular α is due to the increment of crack deflection effect.[16] This may explain the contradictions of the effect of acicular α on fracture toughness. Some authors[2,4,7] reported that the acicular α phase decreases fracture toughness, but other[8–10] have reported the opposite.

As mentioned in the introduction, for conventional $\alpha + \beta$ titanium alloys such as Ti–6Al–4V, furnace-cooling treatment from solutionizing temperature in the $\alpha+\beta$ field produces intergranular β phase containing no or lack secondary phase. However, in the present alloy, similar treatment produces plate-like α within prior β grain, as described above and also in the previous report.[12] The presence of a relatively high β stabilizer in the present alloy seems to suppress the formation of intergranular β during furnace-cooling treatment. Therefore, it can be understood why the fracture toughness of furnace-cooled Ti–6Al–V, in general, is lower than that of an air-cooled one[1] and shows the opposite trend to the present alloy. The presence of plate-like α in FC specimen leads to an increase in fracture toughness by providing crack deflection effect (Fig. 11). The increase of fracture toughness is more pronounced in the microstructure containing very coarse plate-like α by micro cracking and crack branching in addition to the crack deflection as observed in the 1173 FC specimen (Fig 10(c)).

From the above discussion, it can be concluded that the presence of a secondary phase can increase fracture toughness. The increase of fracture toughness is more pronounced when the microstructure contains relatively coarse continuous secondary phase. Both the martensite before testing and the martensite induced by the deformation appear to increase fracture toughness. An exception is found in the microstructure-containing local acicular α where the J_{IC} decreases slightly with the increasing width of acicular α. However, J_{IC} increases monotonously with further increasing of the width of acicular α for the microstructure containing predominantly continuous acicular α. The present study also shows that a relatively better balance of fracture toughness, tensile strength and ductility is given by the microstructure containing coarse plate-like α resulting from furnace-cooling treatment with a cooling rate of around 0.1 K/s from solutionizing temperature. However, a slight decreasing in cooling rate by conducting slow cooling treatment with a cooling rate of around 0.05 K/s instead of furnace cooling treatment causes significant decrease in fracture toughness although almost no change in strength and ductility is found. The decrease of fracture toughness in the microstructure of slow cooled specimen is mainly due to the absence of extrinsic toughening mechanism, which is a result of the absence of a secondary phase.

5. Conclusions

Fracture toughness, J_{IC}, and tensile properties of β-rich $\alpha + \beta$ type Ti–4.5Al–3V–2Mo–2Fe alloy were evaluated in the microstructures containing different types of secondary phases in the matrix β (within prior β grain) resulting from different cooling rates from various solutionizing temperatures in $\alpha + \beta$ field. The following results were obtained.

(1) The types of secondary phases observed in WQ, AC and FC specimens are martensite $\alpha(\alpha'')$, acicular α and plate-like α, respectively. While, SFC specimens have matrix β lacking a secondary phase. Additionally, deformation-induced martensite (α'') is observed in the water-quenched specimens after testing.

(2) The fracture toughness of specimens having a microstructure containing a secondary phase is, in general, superior to that of specimens having a microstructure lacking secondary phase.

(3) Fracture toughness and flow stress of specimens having microstructures containing secondary phases depend strongly on the type and size (width) or volume fraction of the secondary phase.

(4) Both the martensite α before testing and the deformation-induced martensite appear to increase fracture toughness.

(5) J_{IC} appears to decrease slightly with increasing width of acicular α for the microstructure containing predominantly

local acicular α, but increases monotonously with further increasing width of acicular α.

(6) J_{IC} increases significantly with increasing volume fraction or width of plate-like α.

(7) The increase of fracture toughness in the microstructures containing a secondary phase is mainly due to the increasing effect of extrinsic toughening mechanism.

Acknowledgements

The authors would like to thank to Air Force Office of Scientific Research Asian of Aerospace R & D for financial support under Grant No F49620-96-0183 and Japan Titanium Association for encouraging this study.

REFERENCES

1) *Materials Properties Handbook: Titanium Alloys*, ed. by R. Boyer, G. Welsch and E. W. Collings, ASM International, Materials Park, OH, USA, (1994) pp. 1–1060.
2) A. L. Helbert, X. Feugas and M. Clavel: Metall. Mat. Trans. A **30A** (1999) 2853–2863.
3) G. Terlinde, H.-J. Rathjen and K.-H. Schwalbe: Metall. Mat. Trans. A **14A** (1983) 2101–2115.
4) G. Terlinde, H.-J. Rathjen and K.-H. Schwalbe, Metall. Mat. Trans. A **19A** (1988) 1037–1049.
5) M. Niinomi, T. Kobayashi, I. Inagaki and A. W. Thomson: Metall. Mat. Trans. A **21A** (1990) 1733-1744.
6) I. A. Akmoulin, M. Niinomi and T. Kobayashi: Metall. Trans. A **25A** (1994) 1655–1666.
7) L. J. Hunter, M. Strangwood and P. Bowen: *Titanium '95 Science and Technology*, ed. by P. A. Blenkinshop, W. J. Evans and H. M. Flower, The Institute of Materials, London, UK, vol. 2, (1996) pp. 925–932.
8) M. Niinomi, T. Kobayashi and I. Inagaki: Mat. Sci. Tech., **4** (1988) 803–809.
9) M. Niinomi and T. Kobayashi: Mat. Sci. Engng. A **A213** (1996) 16–24.
10) J. C. Williams, F. H. Froes, J. C. Chesnutt, C. G. Rhodes and R. G. Berryman: *Toughness and Fracture Behavior of Titanium*, ed. by J. B. Wheeler *et al*, ASTM STP 651, PA, USA, (1978) pp. 64-114.
11) M. Ishikawa, O. Kuboyama, M. Niikura and C. Ouchi: *Titanium '92 Science and Technology*, ed. by F. H. Froes and I. L. Caplan, TMS, Warrendale, PA, USA, vol. 2, (1993) pp. 141-148.
12) Gunawarman, M. Niinomi, K. Fukunaga, D. Eylon, S. Fujishiro and C. Ouchi: *Proceeding of 2nd ISAEM conference*, Guilin, P. R. China, October 20–21, 2000, Journal of Material and Product, in press.
13) A. Ogawa, K. Minakawa and S. Takagi: *Titanium '95 Science and Technology*, ed. by P. A. Blenkinshop, W. J. Evans and H. M. Flower, The Institute of Materials, London, UK, vol. 2, (1996) pp. 1251–1258.
14) T. Fujita, M. Ishikawa, S. Hashimoto, K. Minakawa and C. Ouchi: *Beta Titanium Alloy in the 1990s*, ed. by D. Eylon, R. R. Boyer and D. A. Koss, TMS, Warrendale, PA, USA, (1993) pp. 61-307.
15) R. R. Boyer, K. Minakawa and A. Ogawa: *Titanium '95 Science and Technology*, ed. by P. A. Blenkinshop, W. J. Evans and H. M. Flower, The Institute of Materials, London, UK, vol. 2, (1996) pp. 933–939.
16) Gunawarman, M. Niinomi, K. Fukunaga, D. Eylon, S. Fujishiro and C. Ouchi: Mat. Sci. Engng. A **A308** (2001) 216–224.
17) ASTM Designation E813-89: Standard test method for J_{IC}, ASTM, Philadelphia, PA, USA, (1996) 633–647.
18) K. Hirano, H. Kobayashi and H. Nakazawa: Journal of Material Testing and Evaluation, **13** (1985) 356–362.
19) R. R. Boyer, R. Bajoraitis and W. F. Spurr: Microstructure, *Fracture Toughness and Fatigue Crack in Titanium Alloys*: ed. by A. K. Chakrabarti and J. C. Chesnutt, TMS, Warrendale, PA, USA, (1987) pp. 149–170.
20) R. D. Briggs: *Advances in the Science and Technology of Titanium Alloy Processing*, ed. by I. Weiss, R. Srinivasan, P. J. Bania, D. Eylon and S. L. Semiatin, TMS, Warrendale, PA, USA, (1997) pp. 413–420.
21) R. K. Bird, T. A. Wallace and W. D. Brewer: *Advances in the Science and Technology of Titanium Alloy Processing*, ed. by I. Weiss, R. Srinivasan, P. J. Bania, D. Eylon and S. L. Semiatin, TMS, Warrendale, PA, USA, (1997) pp. 473–479.
22) Y. Ito, Y. Moriguchi, N. Nagai, A. Harimoto, Y. Tekeda and T. Daikoku: *Titanium '80 Science and Technology*, ed. by H. Kimura and O. Izumi, AIME Warrendale, PA, USA, (1980) pp. 593–600.